THE JOURNAL OF BIOLOGICAL CHEMISTRY VOL. 284, NO. 52, pp. 36109–36117, December 25, 2009
© 2009 by The American Society for Biochemistry and Molecular Biology, Inc. Printed in the U.S.A.

Reversible Cyclosporin A-sensitive Mitochondrial Depolarization Occurs within Minutes of Stroke Onset in Mouse Somatosensory Cortex *in Vivo*

A TWO-PHOTON IMAGING STUDY[*] [S]

Received for publication, August 17, 2009, and in revised form, October 17, 2009 Published, JBC Papers in Press, November 5, 2009, DOI 10.1074/jbc.M109.055301

Ran R. Liu[‡] **and Timothy H. Murphy**[‡§1]

From the [‡]*Department of Psychiatry and* [§]*Brain Research Center, University of British Columbia, Vancouver, British Columbia V6T 1Z3, Canada*

Neuronal structure and function are rapidly damaged during global ischemia but can in part recover during reperfusion. Despite apparent recovery in the hours/days following an ischemic episode, delayed cell death can be initiated, making it important to understand how initial ischemic events affect potential mediators of apoptosis. Mitochondrial dysfunction and the opening of the mitochondrial permeability transition pore (mPTP) are proposed to link ischemic ionic imbalance to mitochondrially mediated cell death pathways. Using two-photon microscopy, we monitored mitochondrial transmembrane potential ($\Delta\psi_m$) *in vivo* within the somatosensory cortex during ischemia and reperfusion in a mouse global ischemia model. Our results indicated a synchronous loss of $\Delta\psi_m$ within 1–3 min of ischemic onset that was linked to within seconds of plasma membrane potential ($\Delta\psi_p$) depolarization. $\Delta\psi_m$ recovered rapidly upon reperfusion, and no delayed depolarization was observed over 2 h. Cyclosporin A treatment largely blocked $\Delta\psi_m$ collapse during ischemia, suggesting a role for the mPTP. Blocking $\Delta\psi_m$ depolarization did not affect structural damage to dendrites, indicating that the opening of the mPTP and damage to dendrites are separable pathways that are activated during $\Delta\psi_p$ depolarization. Our findings using *in vivo* imaging suggest that mitochondrial dysfunction and specifically the activation of the mPTP are early reversible events during brain ischemia that could trigger delayed cell death.

Ion and water imbalance during stroke are widely accepted as chief contributors to acute ischemic injury, but how these events are linked to more slowly activated cell death pathways is unclear (1). Neurons within the cortex and the hippocampus can recover both structure and function within hours after brief ischemia (2, 3) but are still subject to cell death with apoptotic features days later (4). One mechanism described *in vitro* that may link intracellular Ca^{2+} elevation to cell death pathways is the activation of mitochondrial permeability transition pore (mPTP)[2] in response to mitochondrial Ca^{2+} overload (5–8). mPTP activation can lead to mitochondrial transmembrane potential ($\Delta\psi_m$) collapse and excessive reactive oxygen species generation (5, 7, 9). Mitochondrial dysfunction, and specifically mPTP opening, has been suggested to contribute to ischemic injury (10, 11), although its exact role and timing are unclear. *In vitro* studies in neurons suggest that mitochondrial dysfunction occurs during ischemia and excitotoxic ion overload (5, 7, 12–15); however, other evidence suggests that mitochondrial dysfunction may be delayed and occur during reperfusion or after a period of ionic stress (9, 16, 17). To complicate matters, there are differences between conditions during *in vitro* ischemia-like events and stroke *in vivo* (2, 13). Previously, the role of mitochondrial dysfunction has been addressed in stroke *in vivo* using end point measures of histological and biochemical markers (8, 16) or using potentially less direct methods such as NADH fluorescence time-lapse imaging (18). To date, no real-time monitoring of mitochondrial function *in vivo* during stroke and reperfusion has been performed. Consequently, when and where mitochondrial dysfunction occurs *in vivo* during stroke are unclear.

Here, bilateral occlusion of the common carotid arteries (CCAs) was used to produce rapid and reversible forebrain ischemia (2). When combined with two-photon imaging of rhodamine 123 (Rh123) fluorescence, this model allowed us to monitor $\Delta\psi_m$ with high temporal and spatial resolution. We show that cyclosporin A (CsA)-sensitive mitochondrial depolarization that is indicative of mPTP activation occurs within minutes of ischemic onset in parallel with plasma membrane potential ($\Delta\psi_p$) depolarization.

EXPERIMENTAL PROCEDURES

Animals—Urethane-anesthetized 2–5-month-old green fluorescent protein (GFP-M) and yellow fluorescent protein (YFP-H) transgenic mice (19) and C57BL/6 wild-type mice were used. All mice were bred at the University of British Columbia animal facilities. All experimental anesthesia was

* This work was supported by a grant-in-aid from the Heart and Stroke Foundation of British Columbia and Yukon (to T. H. M.) and grants from the Canadian Stroke Network (to T. H. M.).

[S] The on-line version of this article (available at http://www.jbc.org) contains supplemental Figs. 1–5 and Movies 1 and 2.

[1] To whom correspondence should be addressed: Dept. of Psychiatry, University of British Columbia, 4N1-2255 Wesbrook Mall, Vancouver, BC V6T 1Z3, Canada. Fax: 604-822-7981; E-mail: thmurphy@interchange.ubc.ca.

[2] The abbreviations used are: mPTP, mitochondrial permeability transition pore; $\Delta\psi_m$, mitochondrial transmembrane potential; CCA, common carotid artery; Rh123, rhodamine 123; CsA, cyclosporin A; $\Delta\psi_p$, plasma membrane potential; GFP, green fluorescent protein; EEG, electroencephalogram; ACSF, artificial cerebrospinal fluid; FCCP, carbonyl cyanide *p*-trifluoromethoxyphenylhydrazone; ROI, region of interest; DC, direct current; AC, alternating current; ANOVA, analysis of variance.

achieved by intraperitoneal injections of urethane (0.12%, w/w) as described (20). The core temperature was maintained at 37 ± 0.5 °C using a heating pad with feedback regulation from a rectal temperature probe. A heat exchanger was used to warm the head plate and the area around the craniotomy, including the physiological solution surrounding the water immersion objective. Cortical surface temperature was maintained at ~37 °C by pumping 38 °C water through the heat exchanger using a heating pad water pump (T/Pump TP500, Gaymar, Orchard Park, NY). Urethane supplementation for maintenance of anesthesia and saline injections with glucose for hydration and nutrition were administered as described previously (2). Experimental protocols were approved by the University of British Columbia Animal Care Committee.

Surgery and Imaging Procedures—Mice were attached to a custom-made head hold, and a cranial window was created over the forelimb-hind limb somatosensory cortex. Imaging was performed in the forelimb area in brain regions lacking major arterioles and anterior and lateral to the hind limb border. Detailed surgical procedures for cranial window preparation for *in vivo* two-photon imaging are as described previously (20). Because of the potential low blood-brain barrier permeability of CsA (21) and the reduced ability of Rh123 to penetrate a healthy dura (observed in our experiments), the dura was removed from all preparations to permit direct application of compounds to the cortex. Instrumentation for two-photon laser scanning and the procedure for image acquisition are as described previously (2). During imaging of ischemia, fluorophores were excited at 900 nm because of excitation wavelength requirements of GFP/yellow fluorescent protein. During imaging of pressure injection of KCl and other solutions, all fluorophores were excited at 810 nm because of excitation wavelength requirements for Alexa 594. The Rh123 signal was adequate at both wavelengths (higher signals were observed at 810 nm). For all *in vivo* time-lapse imaging performed during stroke experiments, multiple *z*-series of 20 images with *z*-spacing of 1 μm were taken during ischemia and reperfusion within the superficial dendritic tuft. Each image was the average of three frames taken over 5.5 s. For pressure injection experiments, each frame was taken over 0.46 s, and a total of 50 frames of the same *z*-plane were taken per injection. Pressure injection was triggered at frame 10 after 4.6 s.

CCA Occlusion and Stroke Induction—Fig. 1*A* provides a schematic overview of a CCA occlusion experiment. One suture (5-0, silk, Ethicon, Somerville, NJ) was surgically looped around each CCA as described previously (2). However, the sutures were not crossed over the trachea as performed previously (2). We found that animals with uncrossed sutures had reduced rates of heart failure during stroke, possibly because of reduced pressure on the carotid bodies at the CCA bifurcation. Sutures were pulled by hand to apply pressure on the CCAs, secured with tape to induce occlusion, and released for reperfusion. As observed previously, ischemic durations of >7 min led to poor cardiovascular recovery during reperfusion and were avoided (2). Over the duration of the stroke, two-photon imaging of Texas Red-dextran confirmed that blood flow was blocked immediately upon occlusion of the CCAs and remained occluded for the duration of the stroke (see Fig. 1, *B* and *C*) and detailed previously (20). Our previous two-photon measurements indicated that the CCA occlusion is sufficient to generate a >90% reduction in cortical blood flow within seconds of tensioning the sutures (2). In some animals, a second stroke was induced. For measurements of Rh123 fluorescence or electroencephalogram (EEG) quantification, both first and second stroke trials were pooled for our final data comparison (see Figs. 2 and 4). Comparison of data from the first and second strokes indicated no significant difference ($p > 0.05$), suggesting that pooling of two stroke trials within the same animal is reasonable. For dendritic structural analysis (see Fig. 5), only the first stroke from each animal was tabulated because some animals never recover completely within the time of monitoring.

Rh123 Application—Rh123 fluorescence was used to estimate $\Delta\psi_m$. Rh123 is concentrated by the mitochondria because of the negative $\Delta\psi_m$, and at a high local concentration, Rh123 fluorescence becomes autoquenched. Upon $\Delta\psi_m$ collapse, it is dispersed and becomes dequenched, leading to an increase in fluorescence. A stock solution of Rh123 (52.5 mM) was made in anhydrous Me_2SO and diluted in HEPES-buffered artificial cerebrospinal fluid (ACSF) to a working solution of 20 μM. Rh123 was directly applied to the craniotomy for 1 h and washed before imaging. A relatively high concentration of Rh123 was required because it was applied to the brain surface. Lower concentrations led to poor loading and signals.

Pressure Injection—For *in vivo* pressure injection experiments (1–4 s, 3–6 p.s.i.; Picospritzer II, General Valve Corp., Fairfield, NJ), injected solutions were first filtered using a 0.2-μm filter and injected into somatosensory cortex layer I. Agarose and a coverslip were applied over the cranial window prior to pressure injection. The pipette was slowly inserted through the agarose and into the brain. Injection protocols were similar to those described previously (22). The injection pipettes were 4–6 megaohms in resistance. Under the condition with added extracellular Ca^{2+}, standard ACSF (135 mM NaCl, 5.4 mM KCl, 1.0 mM $MgCl_2{\cdot}6H_2O$, 1.8 mM $CaCl_2{\cdot}2H_2O$, 5.0 mM NaHEPES) was used to bath the brain prior to imaging, to make the agarose, and to apply under the water immersion objective for the duration of imaging. Under the condition with no added extracellular Ca^{2+}, a similar ACSF was made; however, in this solution, $CaCl_2$ was substituted with 5 mM $MgCl_2$ (135 mM NaCl, 5.4 mM KCl, 5.0 mM $MgCl_2{\cdot}6H_2O$, 5.0 mM NaHEPES). Under this condition, Ca^{2+}-free ACSF was gently perfused over the surface of the brain for 5 min prior to agarose application. Ca^{2+}-free ACSF was also used to make the agarose and to apply under the water immersion objective.

For control injections, standard ACSF, which contained 135 mM NaCl, was injected. For KCl injections, 135 mM NaCl in the ACSF was substituted with KCl, resulting in a total of 140.4 mM KCl (140.4 mM KCl, 1.0 mM $MgCl_2{\cdot}6H_2O$, 1.8 mM $CaCl_2{\cdot}2H_2O$, 5.0 mM NaHEPES). For all experiments performed under the condition of no added extracellular Ca^{2+}, the injection solution was also made Ca^{2+}-free by substituting $CaCl_2$ with $MgCl_2$ as described above. Carbonyl cyanide *p*-trifluoromethoxyphenylhydrazone (FCCP) was freshly made prior to each experiment. FCCP was initially dissolved in anhydrous Me_2SO at 10 mM and diluted with ACSF for pressure injections. A concentration-

response experiment was performed by injecting different concentrations of FCCP to determine the concentration that resulted in maximal $\Delta\psi_m$ depolarization *in vivo*. Injection of FCCP at 50 μM showed a small Rh123 fluorescence response (~30% increase), whereas injection of FCCP at 200 and 500 μM (supplemental Fig. 1) showed similar apparently maximal responses of ~120%. This suggests that the concentration we selected for the rest of the experiments (200 μM) generates a maximal $\Delta\psi_m$ depolarization. For each animal, one to three injections of each treatment were preformed. In cases in which multiple injections of the same treatment were performed, the results were averaged for that animal.

All pressure injections contained Alexa 594 as a tracer (20 μM). This allowed us to monitor the volume of each injection. All Rh123 fluorescence measurements in pressure injection experiments were performed within a circular region of interest (ROI), with the center oriented at the tip of the pipette and the radius being the distance to the point where the tracer Alexa 594 fluorescence intensity measured was half of the intensity measured at the pipette tip. The plot of Alexa 594 fluorescence change *versus* time (n = 30 total injections) showed faster kinetics than any of the Rh123 fluorescence signals (see Fig. 3*B*). This and other data (sham injection of NaCl) indicate that there was no Alexa 594 bleed-through affecting the Rh123 signals. For each injection, Alexa 594 fluorescence at each time point was divided by the maximal intensity measured within that record to obtain values scaled relative to the maximal increase.

Correcting for Nonspecific Effects of Injection—Because volume addition due to pressure injection can cause a small local mechanical stimulation of the brain, in the same experiments, a series of control injections (n = four animals) were performed. In the control injections, no Rh123 elevation was observed. Moreover, pressure injection resulted in a small decrease in tissue fluorescence (~19%) that was attributed to minor tissue deformation due to the injection volume and the solution possibly washing away Rh123 that was present extracellularly. Consequently, records obtained from all other pressure injection experiments were normalized to the control 135 mM NaCl injection to correct for mechanical stimulation-induced fluorescence changes.

Mitochondrial Transmembrane Potential Imaging and Analysis—In stroke experiments, imaging of Rh123 was done within layer I of the somatosensory cortex, typically within 50 μm of the pial surface. The maintained presence of Rh123 within mitochondria after stroke was confirmed by monitoring basal Rh123 fluorescence at times after reperfusion onset. We were also able to trigger a second Rh123 fluorescence elevation during the second stroke, indicating the presence of responsive dye. In pressure injection experiments, imaging of Rh123 was also done within layer I of the somatosensory cortex, typically within 30–70 μm of the pial surface.

To quantify Rh123 signal changes in stroke experiments, for each time point, fluorescence values (F) during ischemia within a given ROI (typically 80 × 80 μm) were subtracted from base-line values ($dF = F - F_0$). dF values were normalized to base-line values (F_0) to give dF/F_0 values. In pressure injection experiments, for a given time point, the F values within the ROI were subtracted from the base-line average (F_0) to give dF. F_0 was calculated by averaging the F values of a given ROI over the first 10 time-lapse images acquired during the base-line period before injection (recorded over 4.6 s). dF values within an ROI were then normalized to the base line (F_0) to generate dF/F_0 values.

Pharmacology—CsA (C3662, Sigma) was stored in solid form at 4 °C. Immediately prior to an experiment, CsA was dissolved into anhydrous Me_2SO (25 mg/ml) and subsequently diluted in ACSF to a working concentration of 20 μM. CsA at 20 μM was bath-applied directly to the craniotomy for 1 h and mixed into the agarose at 10 μM for sustained application. An FK-506 (F4679, Sigma) stock solution was prepared in anhydrous Me_2SO (20 mg/ml) and stored at 4 °C. During the experiments, it was diluted to a working concentration of 50 μM in ACSF. FK-506 was bath-applied directly to the craniotomy for 1 h and mixed into the agarose at 50 μM for sustained application. Note that concentrations of both CsA and FK-506 within the brain were expected to be lower because the drugs were applied only to the surface. In experiments in which both Rh123 and a drug (such as CsA) were incubated, Rh123 was always incubated first.

EEG Recording—EEG recording was performed as described previously (2). One electrode was inserted into the agarose inside the craniotomy, a second reference on the back between the scapula, and a ground electrode on the foot. A surface direct current (DC) EEG was recorded as described previously (2). Abrupt changes in the DC EEG potential were indicative of $\Delta\psi_p$ depolarization. After alternating current (AC) filtering (0.1–10-Hz band pass) or collection of the EEG in an AC mode, we observed slow wave cortical activity (~1 Hz). The suppression of this slow wave cortical activity was used to define the onset of occlusion (supplemental Fig. 2, *upper*). The appearance of a large slow ripple oscillation on AC EEG recording was temporally correlated with a maximal rate of $\Delta\psi_p$ depolarization (supplemental Fig. 2) (2). In stroke trials that lacked DC EEG recording (because of larger offsets), AC mode recording was used to estimate the time when $\Delta\psi_p$ depolarization reached a maximal rate of depolarization. DC EEG recording was required to determine a measure of the total $\Delta\psi_p$ depolarization amplitude. For this reason, the number of ischemic trials was different between latency from occlusion to maximal rate of $\Delta\psi_p$ depolarization (see Fig. 4*D*) and total $\Delta\psi_p$ depolarization amplitude (see Fig. 4*E*) because some animals had only AC mode recordings. Calcium imaging data in supplemental Fig. 3 was reanalyzed from Ref. 2 (see this article for a full description of this method and data). The MouseOx pulse oximeter (Starr Life Sciences, Oakmont, PA) was used in some animals to monitor heart rate and oxygen saturation and was mounted on the tail (2).

Assessing Changes in Dendritic Morphology during Stroke—The dendritic tufts of GFP-labeled layer V neurons were imaged within 50 μm of the pial surface. CCA occlusion can induce shifts in the vertical position of the cortex, making it difficult to examine only a single image plane. To ensure that we examined the same dendrites throughout the experiment despite small vertical position shifts, z-series of 20 images with z-spacing of 2 μm were taken.

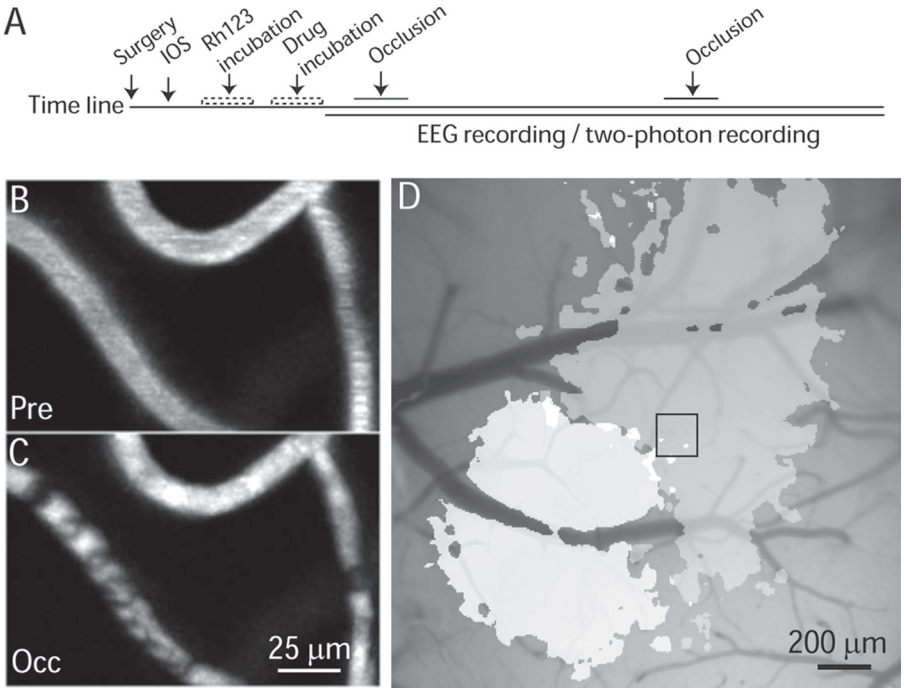

FIGURE 1. **Experimental procedures and monitored parameters.** *A*, experimental schematic. Each incubation was 1 h, and each period of ischemia was ~6.5 min, with 2 h between strokes. In experiments in which both Rh123 and a drug (CsA or FK-506) were incubated, Rh123 was always incubated first. *B* and *C*, examples of two-photon imaging of blood flow using Texas Red-dextran showing before (*Pre*) and immediately after the onset of occlusion (*Occ*). The movement of the red blood cells resulted in regularly spaced horizontal streaks when scanned by the laser and subjected to frame averaging (*B*, *Pre*). Upon occlusion, the movement of the red blood cells significantly slowed down as indicated by stalled flow (*C*, *Occ*). *D*, example of intrinsic optical signal image taken before stroke, showing the sensory representation of the contralateral left forelimb (*darker gray*) and hind limb (*lighter gray*) over the right somatosensory cortex. Two-photon imaging during CCA occlusion was performed in the forelimb representation as indicated by the *black box*. The image shown of the right hemisphere is oriented so the anterior is located up and the lateral to the right.

Intrinsic Optical Signal Imaging—Intrinsic optical signal imaging was performed before stroke to locate the forelimb-hind limb somatosensory cortex so that all two-photon imaging could be done in the posterior region of the forelimb representation (see Fig. 1*D*). The intrinsic optical signal imaging recording procedures and instrumentation used were as described previously (2). Contralateral forelimb and hind limb functional maps were recorded at a focus depth of 200 μm below the cortical surface.

Image Analysis—Image analysis was done with ImageJ software. Image filtering and dendritic bleb quantification were done as described previously (2). For Rh123 fluorescence intensity analysis, the fluorescence percent change from the base line (dF/F_0) was calculated for each time point within a given ROI as described above.

Statistics—Statistical analysis comparing two groups was made by *t* tests. One-way analysis of variance (ANOVA) was used when comparing repeated measures within the same group (time course data) followed by a post hoc Bonferroni multiple comparison test. When comparing repeated measures between two groups, a two-way ANOVA was used.

RESULTS

Mitochondrial Depolarization during Global Ischemia—To address the role of $\Delta\psi_m$ depolarization during stroke, we performed *in vivo* imaging within the mouse forelimb somatosensory cortex (Fig. 1, *A–D*). CCAs were occluded bilaterally for ~6.5 min, resulting in a reduction in cortical blood flow (Fig. 1, *B* and *C*) (2). Within 2 min of stroke induction, a massive $\Delta\psi_p$ depolarization occurred (within 91 ± 12 s, n = 15 ischemic trials). To demonstrate that this $\Delta\psi_p$ depolarization detected by the DC EEG was closely associated with local ionic influx, intracellular Ca^{2+} influx and dendritic structural changes were examined during stroke. All three events showed close temporal correlations with each other (supplemental Fig. 3). Rh123 was applied to the cortex to monitor $\Delta\psi_m$ as an indicator of mitochondrial function (Fig. 2*A*) (23). Within two-photon images (Fig. 2*B*), a high density of labeled mitochondria was observed, making it difficult to unequivocally measure the fluorescence of individual mitochondria over time. However, in particular examples, we could observe mitochondrial labeling patterns that were persistent throughout the experiment (indicated by *arrows* in Fig. 2*B*). To reduce variability due to assessing small structures, we quantified the fluorescence of ROIs. During stroke, synchronous $\Delta\psi_m$ collapse occurred within minutes after occlusion (average of 86 ± 11 s, n = 14 ischemic trials) as indicated by a rapid Rh123 fluorescence elevation (135 ± 20% above the base line, n = 14 ischemic trials, maximal amplitude) (Fig. 2, *A* and *B*). The $\Delta\psi_m$ collapse coincided with $\Delta\psi_p$ depolarization (Fig. 2*C*) and occurred 6 ± 4 s before the time point when the $\Delta\psi_p$ depolarization reached the maximal rate (n = 14 ischemic trials) (Fig. 2, *A* and *C*).

Contrary to the hypothesis of $\Delta\psi_m$ depolarizing at reperfusion and contributing to reperfusion injury (9, 11, 16, 17), $\Delta\psi_m$ repolarization occurred rapidly after reperfusion onset (fluorescence reduced by 63% from the maximal increase 145 ± 53 s after reperfusion onset, n = 11 ischemic trials) as indicated by a sharp drop in Rh123 fluorescence that remained at the base line for the entire duration of monitoring, usually for up to 2 h after stroke (Fig. 2*A*). The kinetics of $\Delta\psi_m$ repolarization were similar to the recovery of intracellular Ca^{2+} levels and preceded the recovery of dendritic blebbing, which occurred over 13–41 min (2).

After reperfusion, $\Delta\psi_m$ depolarization could be retriggered by a second stroke (~120 min later), resulting in a similar fluorescence elevation (first stroke, 140 ± 31% above base line, n = seven ischemic trials; second stroke, 132 ± 29% above base line, n = seven ischemic trials; p = 0.85) (Fig. 2*D*). This result indicates that the reduction in fluorescence during reperfusion is reflective of $\Delta\psi_m$ repolarization and not dye loss or bleaching.

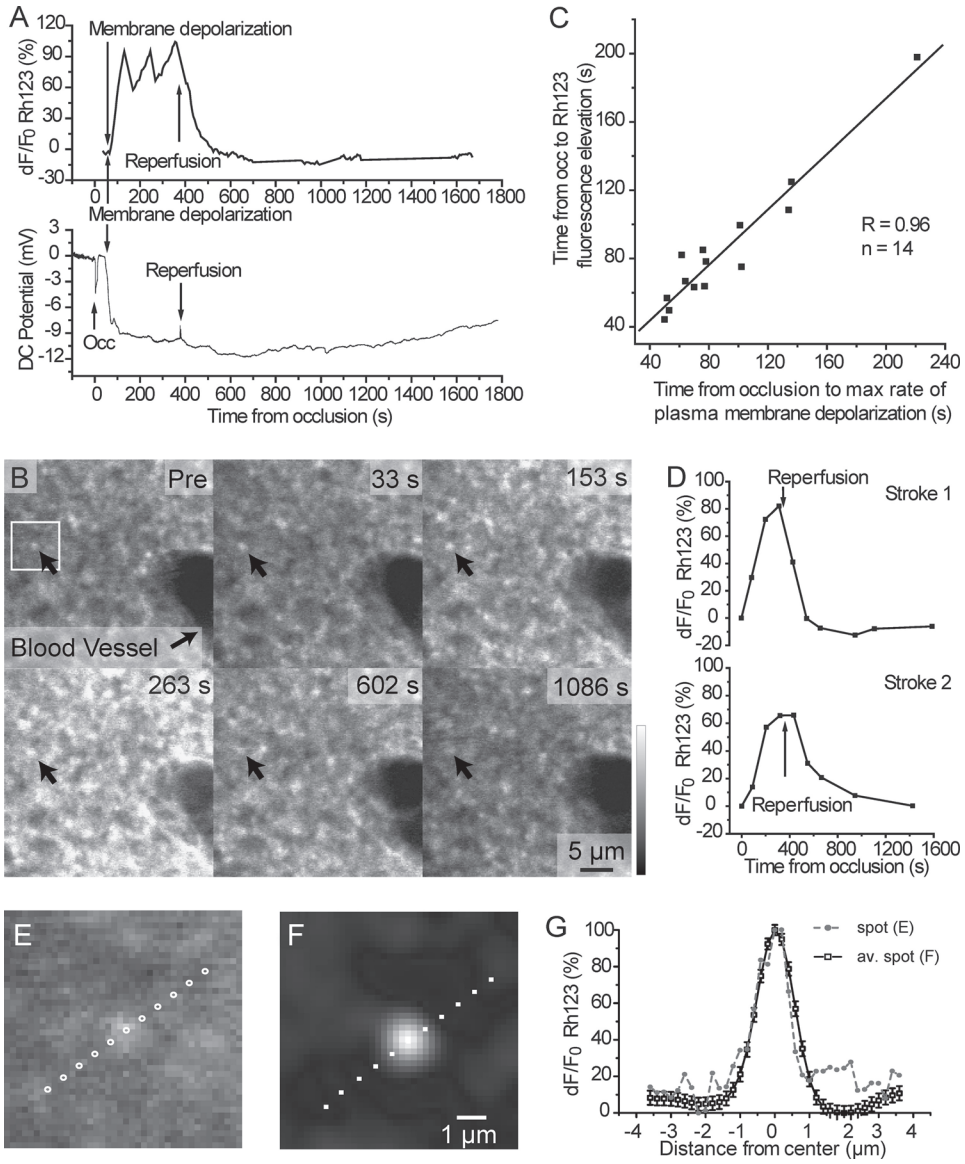

FIGURE 2. **Synchronous $\Delta\psi_m$ collapse occurs during ischemia and coincides with the $\Delta\psi_p$ depolarization.** *A*, *B*, and *D* are recorded from the same animal. *A*, *upper panel*, percent change in Rh123 fluorescence from the base line recorded before ischemia (dF/F_0) within layer I <50 μm from the pial surface. *Lower panel*, the cortical DC EEG recording is shown on the same time scale. *B*, two-photon images (2-μm sections) of Rh123 fluorescence at the indicated times before (*Pre*), during, and after ischemia. In this animal, reperfusion occurred at t = 371 s. *Arrows* indicate mitochondrion-type labeling, and a single mitochondrion is visible pre-stroke and during ischemia and reperfusion. *C*, linear correlation plot of the latency from the time of ischemic onset to the onset of Rh123 fluorescence elevation *versus* the time point when $\Delta\psi_p$ depolarization reached the maximal rate of depolarization (n = 14 ischemic trials, R = 0.96). *occ*, occlusion. *D*, graph of two strokes triggered in the same animal 2 h apart, evoking similar Rh123 fluorescence elevations. *E*, close-up image of the Rh123-stained mitochondrion shown in the box in *B*. *F*, average image of 56 aligned mitochondria from Rh123 images taken from the same animal. *G*, plot of the change in Rh123 fluorescence made from a line profile through the average (*av.*) spot (*F*) or the individual image (*E*). Gaussian fitting of the average Rh123 profile indicated a spot width at a half-maximal intensity of 1.2 μm and an average of 1.1 ± 0.5 μm for n = four mice studied.

The result also suggests that a possible secondary delayed $\Delta\psi_m$ depolarization would have been detectable.

We also created movies of Rh123 fluorescence taken during *z*-stacks before stroke (supplemental Movie 1) and during stroke (supplemental Movie 2). In these movies, we indicate the DC potential to show the relationship between mitochondrial and ischemic depolarization. Importantly, analysis of the Rh123-labeled structures indicated that they were 1.1 ± 0.5 μm in diameter (n = 205 mitochondria from four animals), a size expected for mitochondria given the resolution limits of *in vivo* two-photon microscopy (Fig. 2, *E*–*G*).

To determine whether Rh123 signals may also reflect $\Delta\psi_p$ depolarization as suggested by mathematical modeling (24), we depolarized layer I cortex directly using 140 mM KCl pressure injection (1–4 s) without added extracellular Ca^{2+} to produce $\Delta\psi_p$ depolarization but minimal Ca^{2+} influx and observed no significant Rh123 fluorescence elevation (n = four animals, average peak = 7 ± 1%; p = 0.57 by two-way ANOVA) (Fig. 3, *A* and *B*). With extracellular Ca^{2+}, KCl injection produced a small variable Rh123 signal (n = four animals, average peak = 31 ± 13%; p = 0.07) (Fig. 3*B*). Pressure injection of a 135 mM NaCl solution was used to correct for small nonspecific effects of injection (Fig. 3*A*). To confirm the responsiveness of Rh123 to $\Delta\psi_m$ depolarization and to determine its maximal magnitude, 200 μM FCCP was injected and led to a Rh123 signal comparable with that obtained from ischemia (n = six animals, average peak = 119 ± 17% above base line; p < 0.001 by two-way ANOVA) (Fig. 3, *A* and *B*). These control experiments indicate that Rh123 can respond to changes in $\Delta\psi_m$ depolarization under the conditions we have used and suggest that stroke-related signals were near maximal.

Sensitivity of Mitochondrial Depolarization to CsA during Global Ischemia—In vitro studies suggest that the mPTP contributes to the collapse of $\Delta\psi_m$ during excitotoxic ion overload (5, 7, 11, 14). The mPTP inhibitor CsA was applied within the craniotomy to assess the role of mPTP in $\Delta\psi_m$ collapse during ischemia (25). To demonstrate that CsA does not interfere with mitochondrial Rh123 retention, we injected the uncoupler FCCP post-CsA application and observed a Rh123 signal comparable with that in untreated animals, confirming Rh123 responsiveness (supplemental Fig. 4). During ischemia, CsA treatment largely abolished $\Delta\psi_m$ collapse as evident by the absence of Rh123 fluorescence elevation: n = 11 (control) *versus* n = six (CsA) ischemic trials (p < 0.0001 by two-way ANOVA) (Fig. 4*A*) and n = 14 stroke trials (control) *versus* n = six ischemic trials (CsA) (p = 0.001 by t test) (Fig.

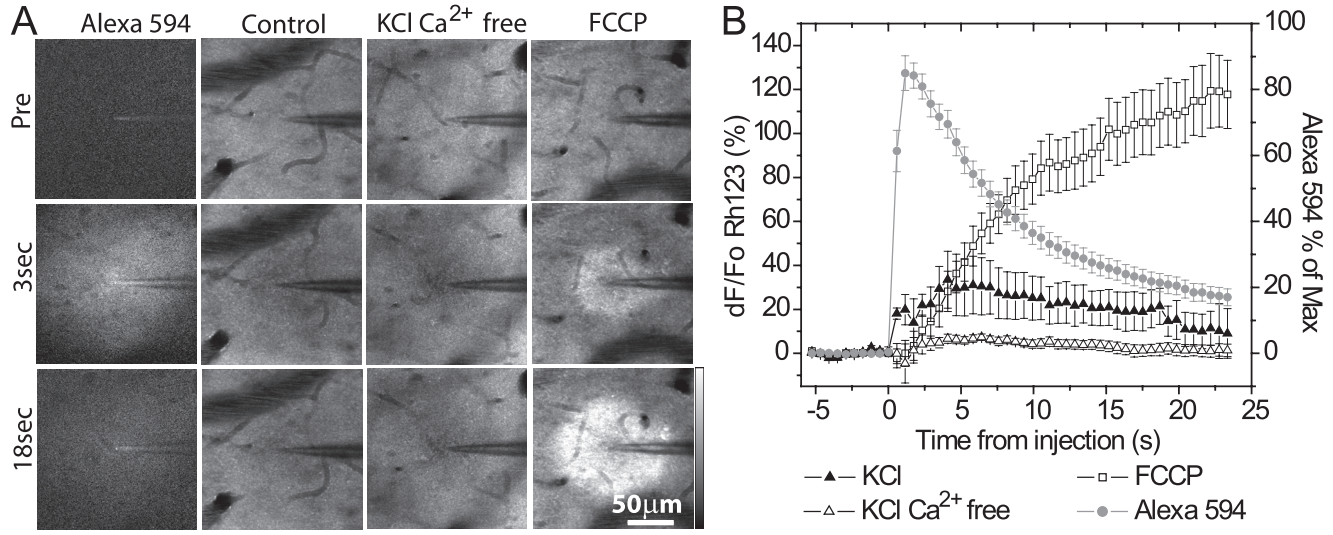

FIGURE 3. **$\Delta\psi_p$ depolarization does not evoke a Rh123 fluorescence elevation.** *A*, two-photon images of Alexa 594 (*left column*) and Rh123 fluorescence (*right columns*, three different treatments) at time points before (*Pre*) and after the start of injection of the indicated solutions. *B*, *left axis*, percent change in Rh123 fluorescence from the base line recorded before injection (dF/F_0) within 30–70 μm from the pial surface. Each animal was normalized to a record where a control NaCl-containing solution was injected. *Right axis*, normalized Alexa 594 fluorescence averaged across all injections, which serves as an injection tracer.

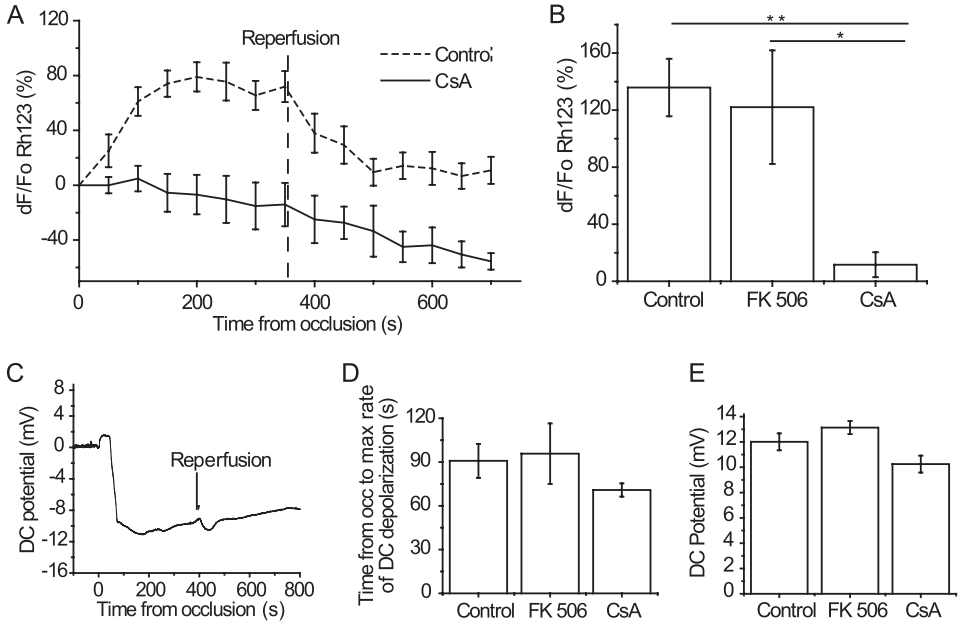

FIGURE 4. **CsA inhibition selectively blocks $\Delta\psi_m$ depolarization during transient global ischemia.** *A*, Rh123 fluorescence percent change from the base line recorded before ischemia (dF/F_0) and in the presence and absence of 10 μM CsA (control, $n = 11$ ischemic trials, and CsA, $n = $ six; $p < 0.0001$ two-way ANOVA). Each data point was averaged over 50 s. *B*, group data comparing the maximal dF/F_0 percent in Rh123 fluorescence during ischemia (control, $n = 14$ ischemic trials, and CsA, $n = $ six; **, $p = 0.001$ by two-way *t* test). FK-506 treatment (50 μM) had no effect compared with the control (FK-506, $n = $ five ischemic trials; $p = 0.74$). CsA treatment was significantly different compared with FK-506 (*, $p = 0.016$). *C*, example DC filtered EEG recording (bottom; 10-Hz low pass) of $\Delta\psi_p$ depolarization during ischemia in an animal treated with CsA. *D*, group data comparing the latency measured from the start of ischemia to when $\Delta\psi_p$ depolarization reached the maximal rate of depolarization. CsA or FK-506 application did not significantly change the latency of $\Delta\psi_p$ depolarization (control, $n = 13$ ischemic trials, and CsA, $n = 12$ ($p = 0.16$); FK-506 $n = 11$ ischemic trials ($p = 0.83$)). *occ*, occlusion. *E*, group data comparing the total amplitude of $\Delta\psi_p$ depolarization. CsA application slightly reduced the amplitude of the $\Delta\psi_p$ depolarization (control, $n = 11$ ischemic trials, and CsA, $n = 10$; $p = 0.08$ by two-sample *t* test), whereas FK-506 treatment did not ($n = 11$ ischemic trials; $p = 0.20$).

4*B*). Note that in Fig. 4*A*, only animals that survived >5 min after ischemia were plotted and compared by ANOVA. CsA-treated animals did show a small initial Rh123 fluorescence increase (12 ± 9% peak increase, $n = $ six ischemic trials) (Fig. 4*B*). It is conceivable that the effect of CsA was due to calcineurin inhibition. However, FK-506, a calcineurin inhibitor that does not affect the mPTP (26), failed to affect the elevation of Rh123 fluorescence during stroke (FK-506, $n = $ five ischemic trials; $p = 0.74$) (Fig. 4*B*). CsA inhibition of $\Delta\psi_m$ collapse was selective, as ischemia-induced $\Delta\psi_p$ depolarization still occurred with similar latency from occlusion (control, $n = 15$ ischemic trials, and CsA, $n = 12$; $p = 0.16$) (Fig. 4, *C* and *D*). CsA treatment caused a small but non-significant reduction (~15%) in the total $\Delta\psi_p$ depolarization amplitude (control, $n = 11$ ischemic trials, and CsA, $n = 10$; $p = 0.08$), an effect not observed with FK-506 ($n = 11$ ischemic trials; $p = 0.20$) (Fig. 4*E*).

Role of Mitochondrial Depolarization in Dendritic Blebbing during Transient Global Ischemia—We assessed the effect of CsA-induced blockade of $\Delta\psi_m$ collapse on dendritic structural damage by examining the dendritic tufts of layer V neurons using *in vivo* imaging. Within minutes of ischemic induction, apical dendrites were found to rapidly swell and bleb (20) and were quantified as described previously (2). Dendrites blebbed during occlusion at the time of $\Delta\psi_p$ depolarization and recovered during reperfusion (control, $n = $ four animals; $p = 0.006$ by one-way ANOVA) (Fig. 5, *A* and *B*). Animals treated with locally applied CsA ($n = $ four animals; $p = 0.092$) showed no significant reduction in dendritic blebbing compared with controls ($n = $ four animals) during ischemia or

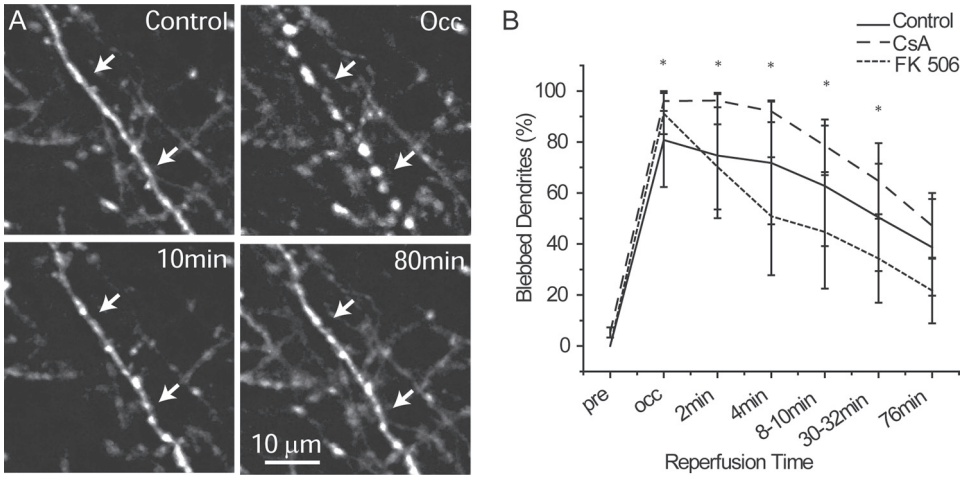

FIGURE 5. **CsA blockade of mitochondrial depolarization during ischemia does not affect dendritic blebbing.** *A*, projection images (4 μm) from a mouse with GFP-labeled dendrites and treated with CsA. *B*, group data comparing dendritic blebbing in CsA-treated, FK-506-treated, and control mice. Dendritic blebs were quantified before occlusion (*pre*), immediately before the reperfusion onset (*occ*), and at time points after reperfusion onset. By assessing non-drug-treated controls, changes in blebbed dendrite percentages during/after stroke were significantly different from before stroke (control, n = four animals; *, $p < 0.05$ by one-way ANOVA). No significant difference in dendritic blebbing in CsA-treated (n = four animals; $p = 0.092$ by two-way ANOVA) or FK-506-treated (n = four animals; $p = 0.462$ by two-way ANOVA) animals was observed compared with controls during stroke.

within 2 h of reperfusion (Fig. 5, *A* and *B*). FK-506, a related molecule that does not affect $\Delta\psi_m$ collapse, was also without effect on ischemic changes to dendritic morphology (n = four animals; $p = 0.462$) (Fig. 5*B*).

DISCUSSION

Mitochondrial Depolarization Is Associated with Stroke Onset and Is Reversible—$\Delta\psi_m$ collapse has been suggested to play a significant role in excitotoxic ion overload (5, 7, 14) and ischemia/reperfusion damage (6, 8, 9, 16, 17). Here, we used Rh123 to monitor $\Delta\psi_m$ in both neurons and glia, which undergo rapid swelling during ischemia *in vivo* (27). During ischemia *in vivo*, $\Delta\psi_m$ collapse occurred with a similar rapid time course as cytoplasmic Ca^{2+} elevation (2), supporting *in vitro* findings that suggest that the two events are closely related (5, 7, 13, 14). *In vitro* studies suggest that the activation of the CsA-sensitive mPTP is associated with delayed Ca^{2+} deregulation and cell death (5, 6, 14, 28). Here, we have shown that *in vivo* CsA-sensitive $\Delta\psi_m$ collapse is reversible. Furthermore, contrary to the prediction that the mPTP would open during reperfusion (because of elevation of reactive oxygen species or Ca^{2+}) (9, 11, 16, 17), our experiments demonstrate that $\Delta\psi_m$ recovers during reperfusion. Perhaps, only brief mPTP opening is sufficient to trigger later cell death.

Mechanisms of Mitochondrial Depolarization and mPTP Involvement—Studies from non-neuronal cells suggest that, during ischemia or ion imbalance, mitochondria depolarize, swell, and release cytochrome c through CsA-sensitive Ca^{2+}-induced mPTP activation (11), with brain mitochondria sharing similar mechanisms (5, 7, 14, 17, 29). However, others have demonstrated that brain mitochondria are relatively resistant to mitochondrial permeability transition evoked by Ca^{2+} overload (30, 31). Some studies have reported that the brain mPTP is relatively CsA-insensitive (31, 32), making the role of CsA-sensitive mPTP activation in ischemic injury unclear (33). These discrepancies may be explained by variation between experimental conditions for mitochondrial isolation, different conditions for *in vivo versus in vitro* experiments, as well as regional or subcellular heterogeneity of mitochondria within the brain. We report that $\Delta\psi_m$ collapse occurs within minutes of stroke onset *in vivo* and is mediated by the activation of a CsA-sensitive mechanism, which suggests mPTP involvement (supplemental Fig. 5).

In vitro and brain slice studies suggest that there are two main events behind $\Delta\psi_m$ depolarization during excitotoxicity. The initial component of $\Delta\psi_m$ depolarization is reported to involve mitochondrial Zn^{2+} uptake (34), mitochondrial Ca^{2+} overload, and depletion of mitochondrial respiratory substrates and is reversible (5), whereas the later component of $\Delta\psi_m$ collapse occurring after ~20 min *in vitro* is associated with mPTP activation (5). Evidence suggests that intracellular Ca^{2+} elevation triggers mPTP opening via binding to cyclophilin D in a CsA-sensitive manner (8, 35). However, alternative CsA-insensitive mechanisms could also promote mPTP opening during ischemia, such as reactive oxygen species release, $\Delta\psi_m$ depolarization, adenine nucleotide depletion, and pH changes (35–37), making it difficult for a single *in vitro* model to mimic *in vivo* stroke parameters.

Rh123 Signals Primarily Reflect $\Delta\psi_m$—There are concerns that the elevation of Rh123 fluorescence during ischemia could in part reflect $\Delta\psi_p$ depolarization (38). We argue that the ischemic CsA-sensitive Rh123 fluorescence signal observed predominately reflects $\Delta\psi_m$. It has been previously reported that CsA can potentially have nonspecific effects aside from mPTP inhibition (11). However, we showed that, during ischemia, CsA selectively inhibited the ischemia-induced Rh123 fluorescence elevation but not ischemic $\Delta\psi_p$ depolarization. This suggests that Rh123 fluorescence elevation largely reflects $\Delta\psi_m$ depolarization, which was abolished by CsA and therefore does not reflect $\Delta\psi_p$ depolarization. We investigated this concern by directly examining the effects of local $\Delta\psi_p$ depolarization on Rh123 signals under non-ischemic conditions using an *in vivo* pressure injection technique. In the absence of added extracellular Ca^{2+}, injection of KCl (140.4 mM) was expected to induce a transient $\Delta\psi_p$ depolarization near the pipette opening close to 0 mV, and yet no Rh123 signals were observed (Fig. 3, *A* and *B*). This suggests that Rh123 fluorescence elevation observed during stroke is reflective of $\Delta\psi_m$ depolarization, not $\Delta\psi_p$ depolarization, and that the two events are dissociable.

As expected during KCl pressure injection in the presence of extracellular Ca^{2+}, a small but variable Rh123 fluorescence increase was seen in solutions containing added extracellular Ca^{2+} but was not observed in the solution lacking added extra-

cellular Ca^{2+} (Fig. 3*B*). This result was consistent with KCl-induced injection leading to a brief $\Delta\psi_p$ depolarization, relatively small Ca^{2+} influx, and a partial $\Delta\psi_m$ depolarization that resulted in a small Rh123 fluorescence elevation. This Rh123 elevation was much smaller than that observed during ischemia (by a factor of 4) likely because, during ischemia, a sustained period of ionic imbalance results in a much greater influx of Ca^{2+}, which subsequently triggers a much larger $\Delta\psi_m$ depolarization.

$\Delta\psi_m$ Depolarization in CsA-treated Animals Induced by Low Oxygen Levels—It is surprising that CsA treatment can block most of the ischemia-induced $\Delta\psi_m$ depolarization. During ischemia, in CsA-treated animals, inhibition of cellular respiration induced by low oxygen levels should induce a small $\Delta\psi_m$ depolarization. Indeed, we did see a small but variable initial Rh123 fluorescence elevation in the CsA-treated animals (Fig. 4, *A* and *B*). However, it is conceivable that $\Delta\psi_m$ depolarization induced by this mechanism could be larger at later time points of ischemia (when the full effects of energy failure are felt), but it does not occur within 6.5 min of global ischemia. It is also possible that, during ischemia, this initial $\Delta\psi_m$ depolarization-induced signal may be masked by small changes in base-line fluorescence that we have previously observed using other probes such as GFP and that were attributed to ischemia reducing the efficiency of imaging (2).

Mitochondrial Depolarization and Dendritic Structural Damage Are Mechanistically Separable—Some studies suggest that CsA is neuroprotective in ischemia models (16, 17). However, because of nonspecific effects of CsA such as calcineurin inhibition (11), it is not clear if the effects are due to mPTP. Our findings indicate that CsA treatment does not result in a measurable reduction in structural damage to dendrites within 2 h after stroke. Indeed, most research on the neuroprotective effects of CsA examined animals at time points days after stroke that may reflect slower apoptotic processes (16, 17). Combined with previous literature (5, 26), our current findings suggest that mPTP inhibition during stroke does not reduce structural damage during occlusion or shortly after reperfusion. However, mPTP opening during ischemia may trigger delayed mechanisms for cell death (supplemental Fig. 5) (17, 28, 39). Interestingly, we have used a focal ischemia model to demonstrate that neurons within the peri-infract zone with beaded dendrites show features of both necrotic and apoptotic cell death pathways by staining for markers of cleaved spectrin and activated caspase (40).

Recent *in vivo* evidence using FK-506 suggested that calcineurin-induced actin depolymerization is the chief mechanism of dendritic blebbing observed after kainate-induced seizures (41). However, using two calcineurin inhibitors (FK-506 and CSA), we did not observe a significant reduction in dendritic structural damage. Conceivably, calcineurin inhibition may selectively affect other aspects of seizure-induced damage.

In summary, combined with previous research, our results indicate that reversible changes in mitochondrial function and synaptic structure and function occur during the first minutes of transient ischemia *in vivo* (2). With prompt reperfusion, dendritic structural abnormalities can exhibit significant recovery (2, 42). However, it is conceivable that, during this time, mitochondrially mediated signals that lead to cell death are initiated, making it important for future neuroprotective treatments to be geared toward both management of acute ion and water imbalances that lead to deranged structure (13, 27, 42, 43) and blocking apoptotic events (39, 44). Importantly, these studies confirm that tools such as CsA that block the brain mPTP *in vitro* (45) also have activity *in vivo* and suggest that these events within the first minutes of stroke onset may be a trigger for later cell death.

Acknowledgments—We thank Pumin Wang and Cindy Jiang for excellent mouse surgeries, Heidi Erb for help with the mouse colony, and Albecht Sigler for assistance with data analysis.

REFERENCES

1. Hossmann, K. A. (2006) *Cell. Mol. Neurobiol.* **26,** 1057–1083
2. Murphy, T. H., Li, P., Betts, K., and Liu, R. (2008) *J. Neurosci.* **28,** 1756–1772
3. Gao, T. M., Pulsinelli, W. A., and Xu, Z. C. (1998) *Neuroscience* **87,** 371–383
4. Yonekura, I., Kawahara, N., Nakatomi, H., Furuya, K., and Kirino, T. (2004) *J. Cereb. Blood Flow Metab.* **24,** 151–158
5. Abramov, A. Y., and Duchen, M. R. (2008) *Biochim. Biophys. Acta* **1777,** 953–964
6. Khaspekov, L., Friberg, H., Halestrap, A., Viktorov, I., and Wieloch, T. (1999) *Eur. J. Neurosci.* **11,** 3194–3198
7. White, R. J., and Reynolds, I. J. (1996) *J. Neurosci.* **16,** 5688–5697
8. Schinzel, A. C., Takeuchi, O., Huang, Z., Fisher, J. K., Zhou, Z., Rubens, J., Hetz, C., Danial, N. N., Moskowitz, M. A., and Korsmeyer, S. J. (2005) *Proc. Natl. Acad. Sci. U.S.A.* **102,** 12005–12010
9. Frantseva, M. V., Carlen, P. L., and Perez Velazquez, J. L. (2001) *Free Radic. Biol. Med.* **31,** 1216–1227
10. Starkov, A. A., Chinopoulos, C., and Fiskum, G. (2004) *Cell Calcium* **36,** 257–264
11. Halestrap, A. P. (2006) *Biochem. Soc. Trans.* **34,** 232–237
12. Abramov, A. Y., Scorziello, A., and Duchen, M. R. (2007) *J. Neurosci.* **27,** 1129–1138
13. Greenwood, S. M., Mizielinska, S. M., Frenguelli, B. G., Harvey, J., and Connolly, C. N. (2007) *J. Biol. Chem.* **282,** 26235–26244
14. Alano, C. C., Beutner, G., Dirksen, R. T., Gross, R. A., and Sheu, S. S. (2002) *J. Neurochem.* **80,** 531–538
15. Rintoul, G. L., Filiano, A. J., Brocard, J. B., Kress, G. J., and Reynolds, I. J. (2003) *J. Neurosci.* **23,** 7881–7888
16. Matsumoto, S., Friberg, H., Ferrand-Drake, M., and Wieloch, T. (1999) *J. Cereb. Blood Flow Metab.* **19,** 736–741
17. Domañska-Janik, K., Buzañska, L., Dluzniewska, J., Kozlowska, H., Sarnowska, A., and Zablocka, B. (2004) *Brain Res. Mol. Brain Res.* **121,** 50–59
18. Mayevsky, A., and Chance, B. (2007) *Mitochondrion* **7,** 330–339
19. Feng, G., Mellor, R. H., Bernstein, M., Keller-Peck, C., Nguyen, Q. T., Wallace, M., Nerbonne, J. M., Lichtman, J. W., and Sanes, J. R. (2000) *Neuron* **28,** 41–51
20. Zhang, S., Boyd, J., Delaney, K., and Murphy, T. H. (2005) *J. Neurosci.* **25,** 5333–5338
21. Uchino, H., Elmér, E., Uchino, K., Li, P. A., He, Q. P., Smith, M. L., and Siesjö, B. K. (1998) *Brain Res.* **812,** 216–226
22. Stosiek, C., Garaschuk, O., Holthoff, K., and Konnerth, A. (2003) *Proc. Natl. Acad. Sci. U.S.A.* **100,** 7319–7324
23. Benel, L., Ronot, X., Mounolou, J. C., Gaudemer, F., and Adolphe, M. (1989) *Basic Appl. Histochem.* **33,** 71–80
24. Ward, M. W., Rego, A. C., Frenguelli, B. G., and Nicholls, D. G. (2000) *J. Neurosci.* **20,** 7208–7219
25. Broekemeier, K. M., Dempsey, M. E., and Pfeiffer, D. R. (1989) *J. Biol. Chem.* **264,** 7826–7830
26. Friberg, H., Ferrand-Drake, M., Bengtsson, F., Halestrap, A. P., and Wieloch, T. (1998) *J. Neurosci.* **18,** 5151–5159

27. Risher, W. C., Andrew, R. D., and Kirov, S. A. (2009) *Glia* **57,** 207–221
28. Precht, T. A., Phelps, R. A., Linseman, D. A., Butts, B. D., Le, S. S., Laessig, T. A., Bouchard, R. J., and Heidenreich, K. A. (2005) *Cell Death Differ.* **12,** 255–265
29. Vergun, O., and Reynolds, I. J. (2005) *Biochim. Biophys. Acta* **1709,** 127–137
30. Andreyev, A., and Fiskum, G. (1999) *Cell Death Differ.* **6,** 825–832
31. Brustovetsky, N., and Dubinsky, J. M. (2000) *J. Neurosci.* **20,** 8229–8237
32. Chinopoulos, C., Starkov, A. A., and Fiskum, G. (2003) *J. Biol. Chem.* **278,** 27382–27389
33. Nicholls, D. G., Vesce, S., Kirk, L., and Chalmers, S. (2003) *Cell Calcium* **34,** 407–424
34. Medvedeva, Y. V., Lin, B., Shuttleworth, C. W., and Weiss, J. H. (2009) *J. Neurosci.* **29,** 1105–1114
35. Basso, E., Fante, L., Fowlkes, J., Petronilli, V., Forte, M. A., and Bernardi, P. (2005) *J. Biol. Chem.* **280,** 18558–18561
36. Halestrap, A. P., Woodfield, K. Y., and Connern, C. P. (1997) *J. Biol. Chem.* **272,** 3346–3354
37. Sheldon, C., and Church, J. (2002) *J. Neurophysiol.* **87,** 2209–2224
38. Nicholls, D. G., and Ward, M. W. (2000) *Trends Neurosci.* **23,** 166–174
39. Cheung, E. C., Joza, N., Steenaart, N. A., McClellan, K. A., Neuspiel, M., McNamara, S., MacLaurin, J. G., Rippstein, P., Park, D. S., Shore, G. C., McBride, H. M., Penninger, J. M., and Slack, R. S. (2006) *EMBO J.* **25,** 4061–4073
40. Enright, L. E., Zhang, S., and Murphy, T. H. (2007) *J. Cereb. Blood Flow Metab.* **27,** 1185–1200
41. Zeng, L. H., Xu, L., Rensing, N. R., Sinatra, P. M., Rothman, S. M., and Wong, M. (2007) *J. Neurosci.* **27,** 11604–11613
42. Li, P., and Murphy, T. H. (2008) *J. Neurosci.* **28,** 11970–11979
43. Andrew, R. D., Labron, M. W., Boehnke, S. E., Carnduff, L., and Kirov, S. A. (2007) *Cereb. Cortex* **17,** 787–802
44. Iyirhiaro, G. O., Brust, T. B., Rashidian, J., Galehdar, Z., Osman, A., Phillips, M., Slack, R. S., Macvicar, B. A., and Park, D. S. (2008) *J. Neurochem.* **105,** 703–713
45. Hansson, M. J., Mansson, R., Mattiasson, G., Ohlsson, J., Karlsson, J., Keep, M. F., and Elmer, E. (2004) *J. Neurochem.* **89,** 715–729

Supplemental fig. 1

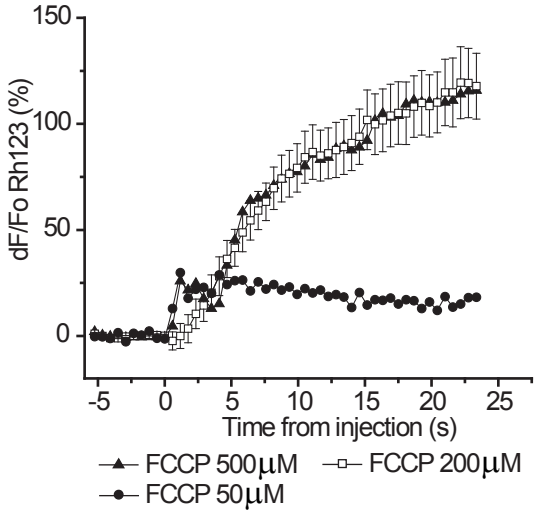

Supplemental fig. 2

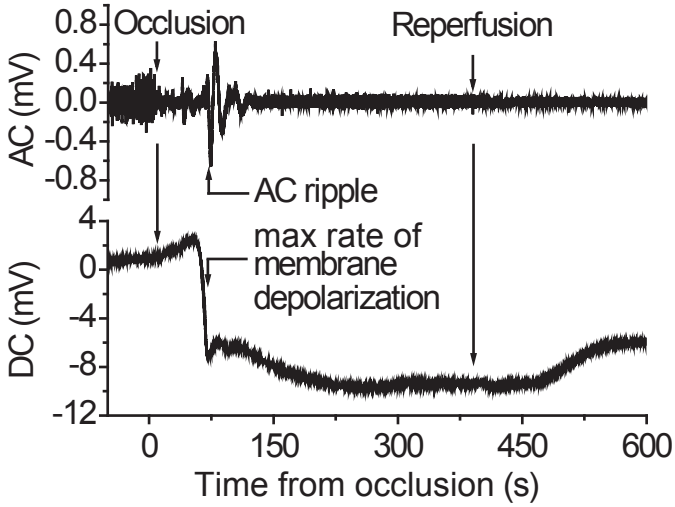

Supplemental fig. 3

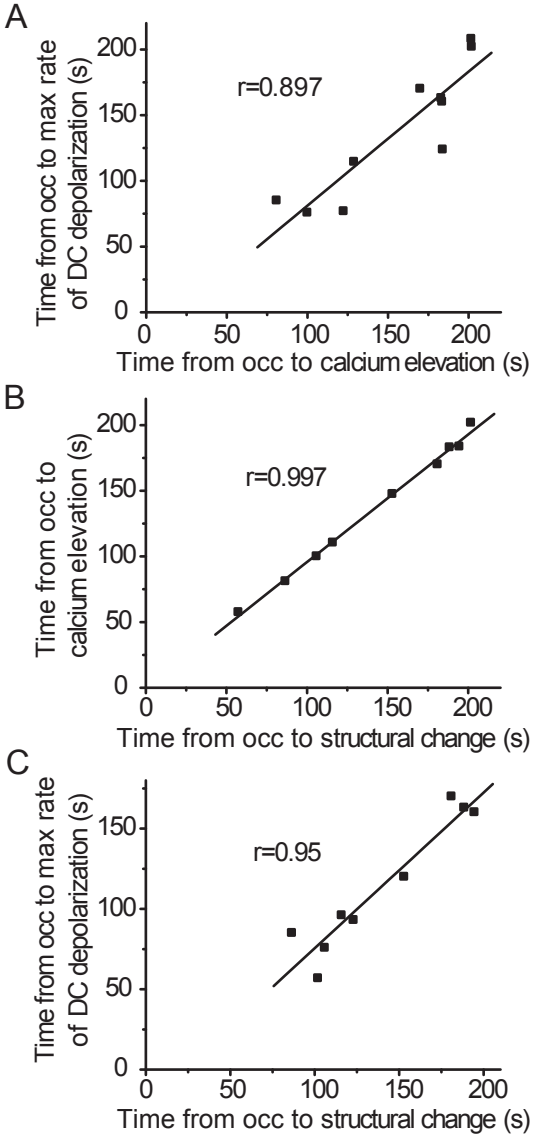

Supplemental fig. 4

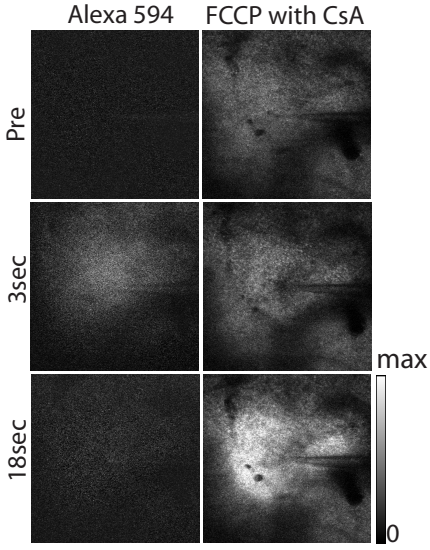

Supplemental fig. 5